Stroke

JOURNAL OF THE AMERICAN HEART ASSOCIATION

American Stroke Association℠

A Division of American Heart Association

Comparative Overview of Brain Perfusion Imaging Techniques

Max Wintermark, Musa Sesay, Emmanuel Barbier, Katalin Borbély, William P. Dillon, James D. Eastwood, Thomas C. Glenn, Cécile B. Grandin, Salvador Pedraza, Jean-François Soustiel, Tadashi Nariai, Greg Zaharchuk, Jean-Marie Caillé, Vincent Dousset and Howard Yonas

The online version of this article, along with updated information and services, is located on the World Wide Web at:

http://stroke.ahajournals.org/cgi/content/full/36/9/e83

Subscriptions: Information about subscribing to Stroke is online at
http://stroke.ahajournals.org/subscriptions/

Permissions: Permissions & Rights Desk, Lippincott Williams & Wilkins, a division of Wolters Kluwer Health, 351 West Camden Street, Baltimore, MD 21202-2436. Phone: 410-528-4050. Fax: 410-528-8550. E-mail:
journalpermissions@lww.com

Reprints: Information about reprints can be found online at
http://www.lww.com/reprints

Comparative Overview of Brain Perfusion Imaging Techniques

Max Wintermark, MD; Musa Sesay, MD; Emmanuel Barbier, PhD; Katalin Borbély, MD, PhD;
William P. Dillon, MD; James D. Eastwood, MD; Thomas C. Glenn, MD; Cécile B. Grandin, MD, PhD;
Salvador Pedraza, MD; Jean-François Soustiel, MD; Tadashi Nariai, MD, PhD; Greg Zaharchuk, MD, PhD;
Jean-Marie Caillé, MD; Vincent Dousset, MD; Howard Yonas, MD

Background and Purpose—Numerous imaging techniques have been developed and applied to evaluate brain hemodynamics. Among these are positron emission tomography, single photon emission computed tomography, Xenon-enhanced computed tomography, dynamic perfusion computed tomography, MRI dynamic susceptibility contrast, arterial spin labeling, and Doppler ultrasound. These techniques give similar information about brain hemodynamics in the form of parameters such as cerebral blood flow or cerebral blood volume. All of them are used to characterize the same types of pathological conditions. However, each technique has its own advantages and drawbacks.

Summary of Review—This article addresses the main imaging techniques dedicated to brain hemodynamics. It represents a comparative overview established by consensus among specialists of the various techniques.

Conclusions—For clinicians, this article should offer a clearer picture of the pros and cons of currently available brain perfusion imaging techniques and assist them in choosing the proper method for every specific clinical setting. (***Stroke***. 2005;36:e83-e99.)

Key Words: computed tomography ■ magnetic resonance imaging ■ tomography, emission computed ■ ultrasonography, Doppler, transcranial ■ perfusion ■ stroke ■ tomography, emission-computed, single-photon

Numerous imaging techniques have been developed and applied to evaluate brain hemodynamics. The main imaging techniques dedicated to brain hemodynamics are positron emission tomography (PET), single photon emission computed tomography (SPECT), Xenon-enhanced computed tomography (XeCT), dynamic perfusion computed tomography (PCT), MRI dynamic susceptibility contrast (DSC), arterial spin labeling (ASL), and Doppler ultrasound. Most of these techniques rely on mathematical models developed at the beginning of the century.[1–4] All these techniques give similar information about brain hemodynamics in the form of parameters such as cerebral blood flow (CBF) or cerebral blood volume (CBV). They use different tracers (diffusible or nondiffusible, endogenous or exogenous) and have different technical requirements. Some are feasible at bedside and others not. The duration of data acquisition and processing varies from one technique to the other. Brain perfusion imaging techniques also differ by quantitative accuracy, brain coverage, and spatial resolu-

tion (Table 1). These differences constitute as many advantages as drawbacks in various clinical settings.

The goal of this article is a comparative overview of the main brain hemodynamics imaging techniques established by consensus among specialists of the different techniques. For clinicians, this should offer a clearer picture of the pros and cons of available brain hemodynamics imaging methods and assist them in choosing the proper technique for every specific clinical setting. The different imaging techniques are presented according to the same template. A technical description, including what kind of contrast is used and whether radiation is involved, is followed by a discussion of the technical requirements. Notably, the duration of a routine study is addressed. Then comes an in-depth discussion of the interpretation of the results, including a description of the underlying mathematical model, the duration of the data postprocessing, the measured parameters, the accuracy of the values in normal parenchymal pixels, in pixels

TABLE 1.   Overview of the Imaging Techniques Dedicated to Brain Hemodynamics

	Brain Perfusion Imaging Techniques						
	PET	SPECT	XeCT	PCT	DSC	ASL	Doppler
Feasibility							
Age range	Adults (and children for static exams)	Adults (and children)	Adults (and children)	Adults (and children)	Adults (and children)	Adults+children	Adults+children
Bedside	No	In some instances	No	No	No	No	Yes
Contrast material	$^{15}O_2$, $C^{15}O_2$, $H_2^{15}O$	^{133}Xe, ^{99m}Tc-HMPAO, ^{99m}Tc-ECD, ^{123}I-IMP (diffusible)	Stable xenon gas (diffusible)	Iodinated contrast material (nondiffusible)	gadolinium chelate (nondiffusible)	None (endogenous contrast)	None (endogenous contrast)
Radiation/study	0.5–2 mSv	3.5–12 mSv	3.5–10 mSv	2–3 mSv	None	None	None
Data acquisition	5–9 min	10–15 min	10 min	40 sec	1 min	5–10 min	10–20 min
Data processing	5–10 min	5 min	10 min	5 min	5 min	5 min	None
Interpretation							
Mathematical model	Kety–Schmidt model	Principle of chemical microspheres for ^{99m}Tc tracers, Kety–Schmidt model for ^{133}Xe and ^{123}I-IMP	Kety–Schmidt model	Meier–Zierler model	Meier–Zierler model	Meier–Zierler model	Other
Assessed parameters	CBV, CBF, rOEF, glucose metabolism	CBF	CBF	CBF, CBV, MTT, TTP, permeability map	CBF, CBV, MTT, TTP, permeability map	CBF	ICA BFV
Large vessels*	No influence on results	No influence on results	No influence on results	Influence results	Influence results	No influence on results	Not applicable
Quantitative accuracy	Yes	Yes for ^{133}Xe and ^{123}I-IMP; no for the others tracers	Yes	Yes	Not in daily practice	Yes	Yes for hemispheric CBF
Including for low perfused areas†	Yes	Not applicable	Yes	Yes	Not applicable	Not <10 mL/min/100 g	Not applicable
Reproducibility	5%	10%	12%	10–15%	10–15%	10%	5%
Brain coverage	Whole brain	Whole brain	6-cm thickness	4–5 cm thickness	Whole brain	Whole brain	One measurement for each hemisphere
Spatial resolution	4–6 mm	4–6 mm	4 mm	1–2 mm	2 mm	2 mm	Not applicable
Minimal time interval between 2 successive exams	10 min	10 min (split-dose technique for ^{99m}Tc-HMPAO, ^{99m}Tc-ECD and ^{123}I-IMP)	20 min	10 min	25 min	0 min	0 min
Clinical applications							
Clinical fields	Chronic cerebrovascular disorders	(Acute and) chronic cerebrovascular disorders	Acute and chronic cerebrovascular disorders	Acute and chronic cerebrovascular disorders	Acute and chronic cerebrovascular disorders	Chronic cerebrovascular disorders	Acute cerebrovascular disorders
		Trauma	Trauma	Trauma		Trauma	Trauma
	Dementia and psychiatric diseases	Dementia and psychiatric diseases	Vasospasm	Vasospasm	Vasospasm	Neurodegenerative disorders	Vasospasm
	Epilepsy	Epilepsy	Epilepsy				
	Brain tumors			Brain tumors	Brain tumors	Brain tumors	
	Brain activation studies	Brain activation studies				Brain activation studies	
Emergency setting	No	In some instances	Yes	Yes	Yes	Yes	Yes

*"Influence of large vessels" is meant to report for which imaging techniques the CBF values in pixels containing large vessels are significantly superior to the capillary CBF values that are of interest.

†"Quantitative accuracy in low perfusion areas" is meant to report which imaging techniques are quantitatively accurate even in case of altered hemodynamics areas, for example, in ischemic areas.

containing larges vessels, and in pathological pixels with altered hemodynamics, and the reproducibility of the technique. The feasibility of the technique in children and at bedside is also addressed, as well as the afforded brain coverage and spatial resolution and the minimal time interval between 2 successive studies. Finally, the typical clinical applications are reported, as well as the availability of the technique in the emergency setting.

<div style="text-align:center">

Positron Emission Tomography
Tadashi Nariai, MD, PhD;
Katalin Borbély, MD, PhD

</div>

Technical Description
PET is a noninvasive diagnostic tool that provides tomographic images of quantitative parameters describing various aspects of brain hemodynamics, including regional CBF (rCBF), regional CBV (rCBV), regional oxygen extraction fraction (rOEF), and cell viability, but also proliferation or metabolic activity of tissues, regional cerebral metabolic rate of oxygen ($rCMRO_2$) or glucose, and neurotransmission processes, etc. These images result from the use of different substances of biological interest labeled with positron emitting radioisotopes (PET radiopharmaceuticals).

The PET tracers used for the measurement of CBF are $^{15}O_2$, $C^{15}O_2$, and $H_2^{15}O$. $H_2^{15}O$ is administered directly by intravenous injection; a 1- to 2-minute scan is performed and its results combined with an arterial blood sampling measurement serving as an input function, and application of the Kety–Schmidt model to this data set leads to quantitative CBF maps.[5,6] $C^{15}O_2$ is inhaled continuously for 8 to 10 minutes, the catalytic action of carbonic anhydrase in the pulmonary vasculature resulting in rapid transfer of the ^{15}O label to $H_2^{15}O$. A 1- to 2-minute scan is performed once a
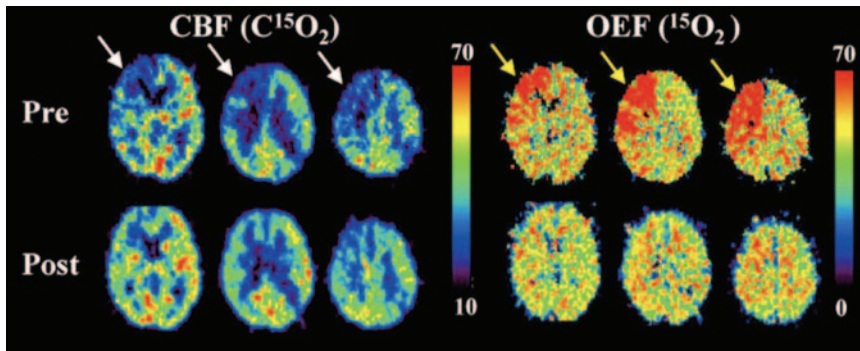
Figure 1. PET CBF and OEF images in a 40-year-old female with moyamoya disease examined before (Pre) and after (Post) a right-side bypass surgery. Before treatment, CBF and OEF are decreased and increased, respectively, in the right frontal region (white arrows), hallmarking poor CVR. CBF and OEF were significantly improved by bypass surgery (yellow arrows).

steady state is reached; the same approach as that described above is used to calculate a quantitative CBF map.[7]

Successive inhalation of $^{15}O_2$, $C^{15}O_2$, and $C^{15}O$ over 60 minutes allows measurement of the rCBV, the rCMRO$_2$, as well as the rOEF, which designates the fraction of the oxygen delivered to brain ($\approx40\%$[3] is extracted by the brain parenchyma and metabolized[8–10]).

^{18}F fluorodeoxyglucose PET can measure the regional glucose consumption of the living tissues and is now widely used for the evaluation of cancer with whole body scanning. Additionally, it is a reliable method to detect a regional metabolic deficit in the brain.[11,12]

PET radiopharmaceuticals are cyclotron products and have a very short half-life (^{18}F 1.7 hours; ^{15}O 2 minutes; ^{13}N 10 minutes; ^{11}C 20 minutes). Whole body radiation exposure by PET examination is usually 0.5 to 2.0 mSv per scan. The radiation dose may differ among institutions depending on the protocol or quality of the PET camera. The duration of the data acquisition depends on the selected method and tracer. It typically ranges ≈5 to 9 minutes for a routine clinical study.

Technical Requirements

In addition to the access to cyclotron PET radiopharmaceuticals, PET imaging requires a PET camera or scanner, usually consisting of several full-ring detectors: BGO (bismuth germanate orthosilicate), lutetium orthosilicate, or gadolinium orthosilicate. Variations on this basic design include partial-ring BGO–dedicated PET scanner and dedicated PET scanner with 6 position-sensitive sodium iodide detectors. A hybrid PET–computed tomography (CT) gives the opportunity for accurate registration and exact correlation of PET functional aspects with anatomical findings. These cameras are much faster ($\approx4\times$) than the older generation of PET cameras.

Interpretation

As described above, PET measurements of CBF are mainly performed using the bolus injection of $H_2^{15}O$ or by the continuous inhalation of $C^{15}O_2$. In both methods, CBF can be quantified based on Kety–Schmidt equation.[10] PET results consist in maps describing CBF, CBV (CBV is calculated from the ratio of the radioactivity in brain to that in peripheral whole blood), rOEF, and rCMRO$_2$ values. Data processing to obtain these maps typically takes 5 to 10 minutes. PET results can be visually interpreted on a computer screen. Correlation with structural information (CT, MRI) is highly desirable for

accurate interpretation.[13] Quantification advantageously completes the visual interpretation and allows to objectively assess changes in postintervention or follow-up studies. The main advantage of PET technique lies in this quantitative accuracy, even in pixels containing large vessels and in brain regions with altered brain perfusion or metabolism. PET results are very reproducible in the current standardized settings.[10,14,15]

Feasibility

PET imaging is feasible in children but is not available at bedside. PET technique affords whole brain coverage. The spatial resolution of PET studies ranges from ≈4 to 6 mm. The minimal time interval between 2 successive examinations is ≈10 minutes for ^{15}O-labeled compound.

Clinical Applications

Because it is not possible in the emergency settings, PET is used mainly in chronic clinical conditions. Chronic cerebrovascular disorders (Figure 1) are the most frequent application of CBF and rOEF measurements. In patients with chronic internal carotid artery (ICA) occlusion, elevated rOEF values are now considered a major key indicator for predicting future impending infarction and determining the indication for bypass surgery.[16–18] Other PET applications are on brain tumors and epilepsy (Figure 2) as well as, to a lesser extent, dementia, movement disorders, and brain activation studies
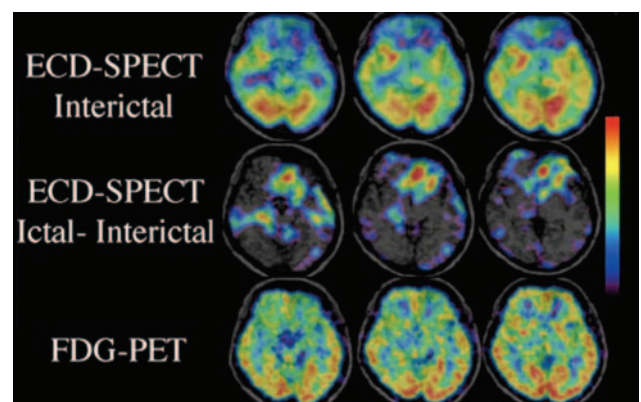

Figure 2. A 42-year-old female with frontal lobe epilepsy. Subtraction of interictal from ictal ^{99m}Tc-ECD SPECT images and coregistration with the patient's MRI identify the epileptic focus more conspicuously than ^{18}F fluorodeoxyglucose (FDG) PET images.

(functional mapping studies).[19] PET may be used for research purposes to validate other brain perfusion methods.[20]

Single Photon Emission CT
Tadashi Nariai, MD, PhD;
Katalin Borbély, MD, PhD

Technical Description

SPECT is a noninvasive technique generating tomographic images of the 3D distribution of a specific radiopharmaceutical, which, depending on its nature, may reflect regional cerebral hemodynamics, dopamine, or other transporter distribution, etc.[21]

[133]Xenon (^{133}Xe) is historically the most important method for measuring brain hemodynamics.[22] However, the gamma rays emitted by ^{133}Xe are of low energy, resulting in abundant scatter and limited spatial resolution. Consequently, retention tracers such as [^{99m}Tc]hexamethylpropylenamine oxime (^{99m}Tc-HMPAO), ^{99m}Tc-Bicisate (ethyl cysteine dimer [ECD]), and ^{123}I inosine–5′-monophosphate (^{123}I-IMP) are more commonly used in clinical SPECT imaging of brain hemodynamics. The doses used in adults are typically 20 milliCuries (mCi) for HMPAO, 30 mCi for ECD, and 5 mCi for ^{123}I-IMP. These activities represent effective doses of 6.88, 12.21, and 3.53 mSv, respectively.

Using retention tracers, the total scan time for a SPECT examination is $\approx$10 to 15 minutes, depending on the imaging device. The goal is to achieve a total of >5 million counts. Compared with step and shoot technique, the continuous acquisition mode may shorten the total scan time and reduce the mechanical wear of the system. Segmentation of the data acquisition into multiple sequential acquisitions allows exclusion of bad data (eg, removing segments of projection data with motion artifacts).

Technical Requirements

Multiple-detector (3- or 4-headed) or other dedicated SPECT cameras for brain imaging should be used for the data acquisition because they afford superior results compared with single- or 2-headed cameras. Use of high-resolution collimation is recommended. The detector pan and zoom capabilities are often used to ensure that the entire brain is included in the field of view while allowing the detector to clear the patient's shoulders.[23]

Reconstruction of 2D images from the projection data collected by the SPECT cameras is usually performed by filtered back projection (FBP). In addition to FBP, different algorithms have been developed to correct for photon attenuation, a possible source of image distortion. The most recent correction techniques are based on measured attenuation maps using transmission scans to reveal an attenuation map specific to each patient. Scattering of the photons in the body of a patient is another important source of error in quantification of activity distribution. The amount of scatter can vary between 10% and 60% of the detected events. Different techniques, such as pulse height analysis, use of multiple energy windows, or deconvolution, allow subtraction of the scatter from the projection data before the image reconstruction. Finally, several iterative reconstruction methods such as

ordered subsets expectation maximization have been proposed recently to correct images for artifacts and noise. Starting from an "initial guessed counts distribution" in the voxel grid or from an already created FBP image, the ordered subsets expectation maximization algorithm elaborates iteratively the image grid, the final end point being to reach a state in which each pixel contains the number of counts it was containing in the raw matrix.[23,24]

Interpretation

Data processing relies on the microsphere principle for the Tc-[99m] tracers and on the Kety–Schmidt model for the ^{133}Xe and ^{123}I-IMP, leading to the calculation of rCBF maps. Data processing typically takes 5 minutes.

The rCBF maps obtained with SPECT can be statistically evaluated compared with the normal control to depict the regions with abnormal perfusion. If SPECT results are fairly reproducible (10% of variability), they are not quantitative in the current standardized settings. Particularly, the uptake of ^{99m}Tc-HMPAO is not linearly related to CBF, requiring special correction.[25] An exception is ^{133}Xe SPECT technique, which uses a single detector positioned over the right lung to measure an arterial input function (AIF) and to calculate quantitative CBF values.

Feasibility

SPECT technique can be used at bedside and is feasible in children. One specific bedside indication for SPECT is seizure. Because SPECT uses a retention tracer for measurement of cerebral perfusion, the radiopharmaceutical can be administered at the moment of the seizure and imaging performed later, after stabilization of the patient, to identify the active epileptic focus.

SPECT affords whole brain coverage. The typical spatial resolution of SPECT studies is 4 to 6 mm. In case of challenges (acetazolamide), ^{133}Xe SPECT examinations can be repeated, and the split-dose technique can be used for ^{99m}Tc-HMPAO, ^{99m}Tc-ECD, and ^{123}I-IMP, with administration of 2 half doses 1 hour apart from each other. The obtained images are subtracted from each other.

Clinical Applications

The main indications for SPECT studies are acute and chronic cerebrovascular diseases and presurgical localization of epileptic foci.

Perfusion SPECT provides valuable information in acute stroke with respect to complications,[26] outcome,[27,28] or choice of treatment strategy.[29] In chronic cerebrovascular disease, SPECT assessment of functional reserve capacity may guide decisions regarding vascular surgery.[30,31]

Ictal SPECT studies (eventually complemented by interictal investigations) are indicated in focal epilepsy for the localization of the epileptic focus before epileptic surgery[32] (Figure 2).

SPECT has also been reported to show abnormalities in head trauma patients[33,34] and in a variety of psychiatric disorders (such as major depression, post-traumatic stress disorder, and schizophrenia) and to afford early detection and differential diagnosis of dementia.[35,36] Perfusion SPECT may

provide helpful information in viral encephalitis (eg, herpes simplex encephalitis), vasculitis, and HIV encephalopathy.[37,38] Finally, SPECT assessment of arrest of cerebral perfusion is an accurate technique to confirm brain death.[39]

Xenon-Enhanced CT
Musa Sesay, MD;
Howard Yonas, MD

Technical Description
XeCT has been used for >20 years to evaluate quantitative CBF in humans.[40] Stable (nonradioactive) Xenon is inhaled and serves as contrast material. The Xenon gas rapidly dissolves in blood, freely crosses the lipid-rich blood–brain barrier, and enters the brain. CBF is calculated by using the modified Kety–Schmidt equation, which integrates the following parameters: the time course of the concentration of Xenon in the blood and brain, and the blood–brain partition coefficient (or lambda) for Xenon.[41] The concentration of Xenon in the brain is measured directly by the CT scanner. The concentration of Xenon in arterial blood is determined indirectly and accurately from the end-tidal Xenon provided that the pulmonary function is not severely impaired.[42] The current technique requires the inhalation of a mixture of Xenon (28%) and oxygen (21% to 60% as clinically indicated) within a data acquisition period of 4.3 minutes.[43] After the acquisition of a baseline scan of the entire head, 4 to 6 contiguous 10-mm-thick levels are selected for CBF measurement. Each level is scanned 6× during the inhalation period, with exact table relocation. At the end of inhalation, Xenon is rapidly washed out from cerebral tissues (half-life ≈40 seconds).

Adverse reactions to stable Xenon-like nausea, reversible alteration of sensorium, or respiratory depression have been reported in <0.1% of cases.[44] In addition, patient motion is a serious limitation to the technique. It can produce artifacts, making interpretation difficult and inaccurate. Head immobilization devices, sedation in some patients, and lowering the Xenon concentration to 28% has lessened the incidence of motion artifacts.[43] Patients with severe respiratory disease, patients with full stomach, ventilated patients with a tidal volume <250 mL, and restless patients who cannot be adequately sedated should be excluded from XeCT studies.

The average radiation dose to the brain from a typical study in an adult ranges from 3.5 to 10 mSv.[45]

Technical Requirements
XeCT technology requires a CT scanner and a Xenon delivery system (ENHANCER, DDP; or XETRON, ANZAI). The latter is a compact and fully mobile unit that can be moved between CT suites. It houses the disposable Xenon gas cylinders. A wall outlet source or an oxygen tank can be used for oxygen delivery. The machine is equipped with continuous monitors of CO_2, O_2, and Xenon integrated within a low-resistance respiratory circuit that is initially open to room air, then partially open and finally closed on using. The later feature is vital for limiting the use of Xenon to <5 L per study. The monitors not only provide a means of maintaining inhaled Xenon and O_2 within 1% of prescribed concentration

but also function as a monitor of apnea. Studies are easily accomplished with a mask or via connection to an endotracheal tube with the patient's volume ventilator being used to maintain ventilation through the enhancer.[43]

The medical-grade Xenon is available and distributed worldwide. However, in the United States, Xenon is not currently approved by the Food and Drug Administration (FDA). The technology is only available at this time under IND (investigational new drug) status.

Interpretation
As mentioned above, XeCT technique relies on the Kety–Schmidt equation to extract from the acquired data quantitative information about CBF and the partition coefficient lambda between blood and tissue.[46] Superimposition of the numerical data on the anatomic image yields a high-resolution (full-width half maximum <4 mm) map of quantitative flow data that is tightly coupled to cerebral anatomy.[47] With the addition of a gray or color scale, the data are converted to a map for visual inspection on which regions of interest (ROIs) can be drawn for rCBF quantitative assessment within a wide spectrum of CBF values (0 to 140 mL/100 g per minute). A confidence map is also produced to demonstrate the effects of any patient motion and other artifacts on the data. The data processing requires ≈10 minutes.

Although the stability of the flow value in a single voxel of 10 mm³ is poor, the reliability of the data from an ROI of >100 voxels is ≈12%. This reliability, despite the pharmacological property of Xenon to directly increase CBF by 20% to 30%, is explained by the fact that nearly all the important flow data are acquired before this flow activation (the latter becomes significant only after 2.5 minutes of inhalation).[48] Reliability is also increased by use of a flow phantom that permits standardization of the data and the calibration of scanners from different manufacturers.

Feasibility
Because of this radiation risk, XeCT in children is only recommended after careful consideration of the potential risks and benefits. XeCT does not afford whole brain coverage, but still, 4 to 6 contiguous 10-mm-thick slices can be evaluated. The minimal time interval between 2 successive examinations is ≈10 minutes. XeCT challenge studies, for example for measuring the vasodilatory response to acetazolamide, can thus be performed in an outpatient setting within 30 minutes[43] (Figure 3).

Clinical Applications
Cerebrovascular disorders are the main clinical application of XeCT, which has the ability to provide measurements of equal validity within the cortex as well as the depth of the brain that can determine proximity to the ischemic threshold.[49] Large clinical series of balloon test occlusion have demonstrated the ability of XeCT to select the patients who require bypass surgery before vascular sacrifice.[50] XeCT has also been shown to be useful in understanding the heterogeneity of flow alterations after closed head injury, providing
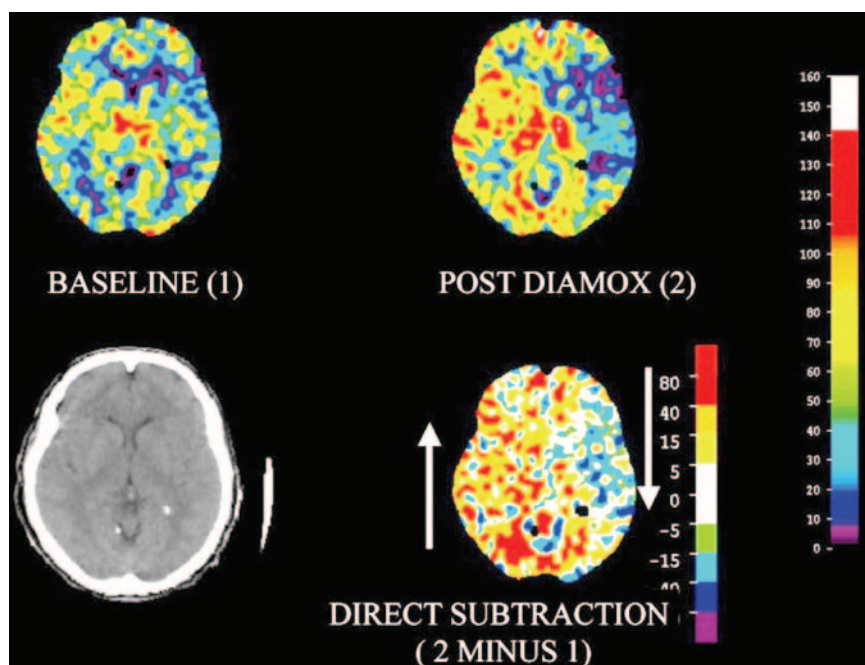
Figure 3. A 40-year-old patient presenting with posture-induced ischemic events ipsilateral to a right carotid occlusion. Comparison of preacetazolamide and postacetazolamide XeCT images demonstrates an increase in rCBF values in the healthy hemisphere only. Subtraction image confirms the existence of a stealing effect with poor CVR predominantly in the left middle cerebral artery territory.

important insights into the efficacy of therapies designed to improve CBF.[51]

As mentioned above, the short half-life of inhaled Xenon makes XeCT CBF particularly adequate for repeat (challenge) tests to study cerebrovascular physiology (Figure 3). Cerebrovascular reserve assessed by examining the quantitative response of flow in patients with occlusive vascular disease has provided a means for identifying high-risk subgroups.[52] The efficacy of blood pressure elevation has been monitored in patients with vasospasm following postsubarachnoid hemorrhage.[53] For patients with elevated intracranial pressure after closed head injury, the ability to monitor the local, regional, and global effects of Pco_2 lowering has provided specific data as to the safety and efficacy of CO_2 manipulation.[54]

Dynamic PCT
James D. Eastwood, MD;
William P. Dillon, MD;
Max Wintermark, MD

Technical Description

Dynamic PCT is a technique for measuring brain hemodynamics that uses first-pass tracer methodology after bolus infusion of intravenous iodinated contrast material. Typically, continuous cine scanning is performed during a total scanning time of 40 to 45 seconds, with a scan rate of 1 image per second. The bolus, typically 40 to 50 cc of 300 to 370 mg/dL iodinated contrast material, is administered via an arm vein.[55]

Although one would expect a higher radiation dose with PCT than standard unenhanced CT, it is necessary to recall that low milliamperes (100 to 150 mA) or kilovolt protocols (80 to 90 kilovolt peaks) are typically used for PCT studies to limit dose. The effective radiation dose involved in a PCT series ranges ≈1.6 to 2.0 mSv (versus 2.5 mSv for a standard unenhanced CT of the brain).[56] Iodinated contrast is safe as

long as not used in patients with renal failure or diabetes mellitus.[57]

Technical Requirements

For adequate PCT data acquisition, a helical CT scanner capable of operating in the cine mode is needed. Multislice CT scanners offer the advantage of greater tissue coverage per acquisition (usually 2 cm) compared with single-slice CT scanners (typically 1 cm). In case of a protocol using 2 successive bolus administrations, a total coverage of 4 to 5 cm can be achieved.[55]

An automatic injector of contrast material capable of at least 3 to 4 cc/second infusion rates is also necessary for an adequate PCT examination to obtain a short bolus. Such an injection rate requires a peripheral venous access with a catheter size of ≥22 gauge (20 or 18 gauge may be optimal).[58]

Interpretation

PCT data processing that can typically be achieved in 5 minutes is performed with postprocessing software using either rate-of-upslope estimation of CBF (for infusion rates above ≈6cc/second) or deconvolution analysis (for infusion rates of 4 to 5 cc/second). Only deconvolution analysis leads to quantitatively accurate results, including in areas with low perfusion.[59] However, PCT technique overestimates brain hemodynamics values in pixels including large vessels.[60]

Ideally, images of CBF, CBV, and mean transit time (MTT) are interpreted together on a workstation permitting the use of visual assessment combined with quantitative analysis with ROIs. Regions of decreased hemodynamics are often represented as regions of prolonged MTT. MTT maps have the property of generally being quite sensitive to the presence of altered brain hemodynamics. Comparing CBF, CBV, and MTT values between abnormal regions and mirror-image control regions is an effective method of measuring the
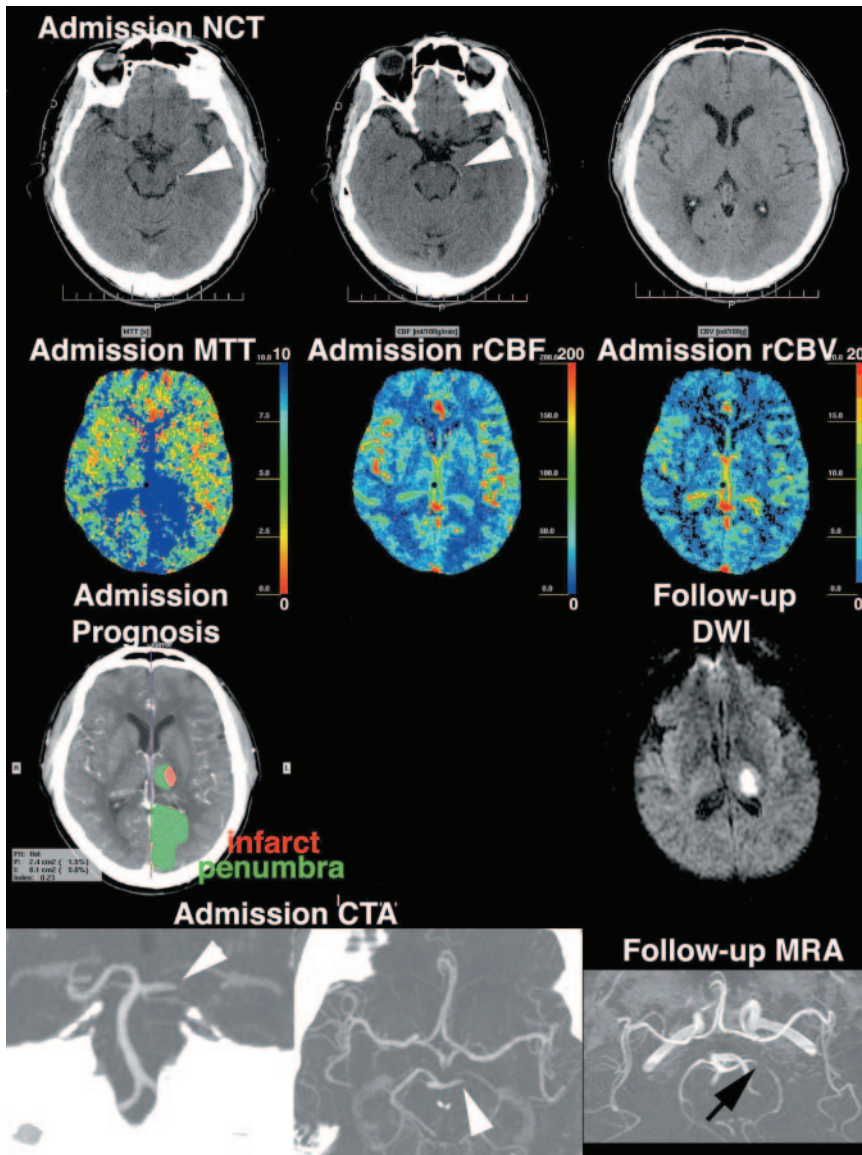
Figure 4. A 55-year-old male patient admitted for right homonymous hemianopsia and right-body sensory loss. The admission noncontrast CT (NCT), obtained 6 hours after symptom onset, was considered unremarkable, except for a dense left posterior cerebral artery (PCA; arrowheads). PCT demonstrates prolonged MTT and reduced rCBF values in the left PCA territory. However, rCBV values are reduced only in a small part of the left thalamus but increased in the rest of the PCA territory. These areas correspond to infarct and penumbra, shown in red and green, respectively. The admission CT angiogram (CTA) demonstrates an occluded left P1 segment that is recanalized but remains focally stenotic on the follow-up MRA obtained 3 days later. The follow-up DWI examination demonstrates a completed stroke in the predicted infarct core in the left thalamus. The penumbra as depicted on the admission PCT did not infarct, most likely as a result of early recanalization.

degree of underperfusion present in a given case or location. Generally, CBF values can be interpreted using thresholds established using other methods, notably XeCT.[61,62] Another way to proceed is to apply the concept autoregulation and to evaluate simultaneously MTT and CBV maps. Within areas with prolonged MTT, the regions with increased CBV resulting from vasodilatation and collateral recruitment are considered to have preserved autoregulation and to represent "tissue at risk," whereas regions with decreased CBV correspond to the infarct core[63,64] (Figure 4).

Feasibility

It is presently not possible to perform a PCT examination at the bedside. The patient must be transported to the CT department.[55]

PCT has a limited spatial coverage (20- to 48-mm thickness). However, the issue of spatial coverage will be addressed in the near future through the development of multislice CT scanners with greater arrays of elements. Even presently, PCT has demonstrated 95% accuracy in the delineation of the extent of supratentorial strokes despite its limited spatial coverage.[65]

The minimal time interval between 2 successive PCT series is 3 to 6 minutes, allowing performance of 2 successive PCT series in the same study to increase spatial coverage and to combine PCT imaging with vasodilatory challenge (eg, acetazolamide challenge).[66]

Clinical Applications

PCT can rapidly detect the size of hypoperfused regions in the setting of acute stroke.[61–64] At the time of this writing, definitions of infarct core and penumbra are undergoing active research to provide understanding of how the method could potentially be used to guide therapy. Anecdotally, in the setting of unilateral carotid occlusion, PCT imaging may be combined with vasodilatory challenge (eg, acetazolamide challenge) to permit identification of tissue at risk for future infarction. Baseline imaging may reveal increased MTT, increased CBV (because of vasodilatation), and decreased CBF. After acetazolamide infusion, further decrease in CBF

is observed in tissue at risk for ischemia without intervention.[66] PCT may be helpful for observing the effects of focal vasospasm after subarachnoid hemorrhage.[67,68]

Finally, PCT can also be used in head trauma patients as a prognostic factor[69] as well as to guide management of intracranial pressure in these patients.[70]

The wide availability of CT scanners in the emergency departments (EDs) and the short duration of PCT examinations make PCT an ideal technique for ED patients, including stroke patients and head trauma patients.[69–71]

Dynamic Susceptibility–Weighted Bolus-Tracking MRI

Cécile B. Grandin, MD, PhD; Salvador Pedraza, MD

Technical Description

DSC relies on the measurement of the T2 or T2* decrease during the first pass of an exogenous endovascular tracer through the capillary bed.[72,73] The technique requires ultrafast imaging, such as echo planar imaging, and principles of echo shifting with a train of observations or spiral imaging. Gradient echo (GRE) or spin echo (SE) sequences can be used, but the signal change measured with GRE (ΔT2*) is greater than that measured with SE (ΔT2), allowing one to use a shorter echo time and a lesser amount of contrast agent. The sequence duration is $\approx$1 minute, and the sampling rate (repetition time of the sequence) should be kept <2 seconds. This can be achieved with GRE sequences for whole brain coverage (up to 24 slices).[74] The used tracer is a conventional chelate of gadolinium, injected through an 18-G catheter into a peripheral vein at a regular dose of 0.1 mmol/kg for GRE or 0.2 mmol/kg for SE, and at an injection rate of 5 to 10 mL/second, immediately followed by a 20- to 30-mL saline flush.[72]

DSC does not expose patients to ionizing radiation. Intolerance to gadolinium chelates is very rare. The contraindications are those of MRI in general: pacemakers and some other implanted metallic or electronic devices or obesity (>150 kg). Fixed ferromagnetic dental devices and intracranial clips generate prominent artifacts. Claustrophobia or agitation may require sedation.

Technical Requirements

Most 1.5-T magnetic resonance (MR) scanners are now equipped with the fast-imaging capabilities required for DSC. The use of a power injector is recommended.

Interpretation

DSC relies on the application of the indicator dilution theory.[4] In case of blood–brain barrier rupture, the indicator dilution theory must be modified, and a measure of the permeability must be introduced.[75,76] For qualitative hemodynamic measurements, a preload dose of contrast before the bolus is an easier way to minimize the effect of contrast leakage.

Using commercially available software, various parameters can be calculated in a few minutes from the time-intensity curves measured in each pixel, allowing one to reconstruct parametric maps. The most commonly calculated parameters are: time to peak (TTP); apparent MTT, corresponding to the first moment of the curves; CBV calculated from the area under the curve; and CBF index, equal to CBV/apparent MTT. These maps do not afford quantitative assessment of brain hemodynamics but provide indicators of hemodynamic disturbances that are very useful in a clinical setting. They can be interpreted visually or semiquantitatively by calculating the ratio or difference between the values in an ROI placed in the abnormal area and a mirror ROI placed in the contralateral area considered as a normal reference. Note that for the moment, there is no standardization in the interpretation of the DSC parametric maps.[77]

The quantification of CBF by DSC requires the deconvolution of the measured tissue curves by an AIF.[78,79] If the AIF is adequately calibrated, absolute quantitative CBV and CBF maps can be obtained.[80] This step is more complex with DSC than with PCT because the relationship between the signal intensity and the gadolinium concentration is not always linear.[81] Several studies have demonstrated a good correlation between the absolute CBV and CBF values obtained according to this approach compared with PET or XeCT.[82–84] Note that to interpret the DSC perfusion maps quantitatively or semiquantitatively, it is necessary to mask out the large vessels (very prominent with GRE sequences). Low perfusion values can be accurately measured until 8 mL/minute per 100 g. Under this level, the signal-to-noise ratio becomes too low for a precise quantification.[85] The reproducibility of the method ranges $\approx$10% to 15%.[86]

Feasibility

DSC has no age limitation and can be performed on children. MRI is not a bedside technique. It is not available at night and during weekends in many institutions.

A spatial resolution $\approx$1.5$\times$1.5$\times$4 mm is routinely available, but the actual in-plane resolution is usually closer to 2 mm, considering the degradation of the point-spread function during the bolus passage.[73]

A delay of 25 minutes between successive contrast injections has been shown to be sufficient for repeated CBF measurements, allowing one to assess the CVR. This delay may be longer for successive CBV measurements.[86,87]

Clinical Applications

The main clinical applications of DSC are acute stroke, chronic cerebrovascular disease, and tumors.

MRI can be performed in the emergency setting of hyperacute stroke. DSC is used in association with diffusion-weighted imaging (DWI) and MR angiography (MRA) for the early evaluation of stroke patients. Prolonged TTP and MTT values are the most sensitive features to detect a hemodynamic disturbance. CBV and CBF maps are more difficult to visually interpret (especially in white matter) but better reflect brain perfusion.[88–90] A threshold can be applied to DSC maps to identify the area at risk for infarction and predict outcome, but no consensus has been achieved regarding the specific thresholds that might distinguish reversible and irreversible ischemia.[91,92] The presence of a mismatch (DSC abnormality larger than the diffusion abnormality),
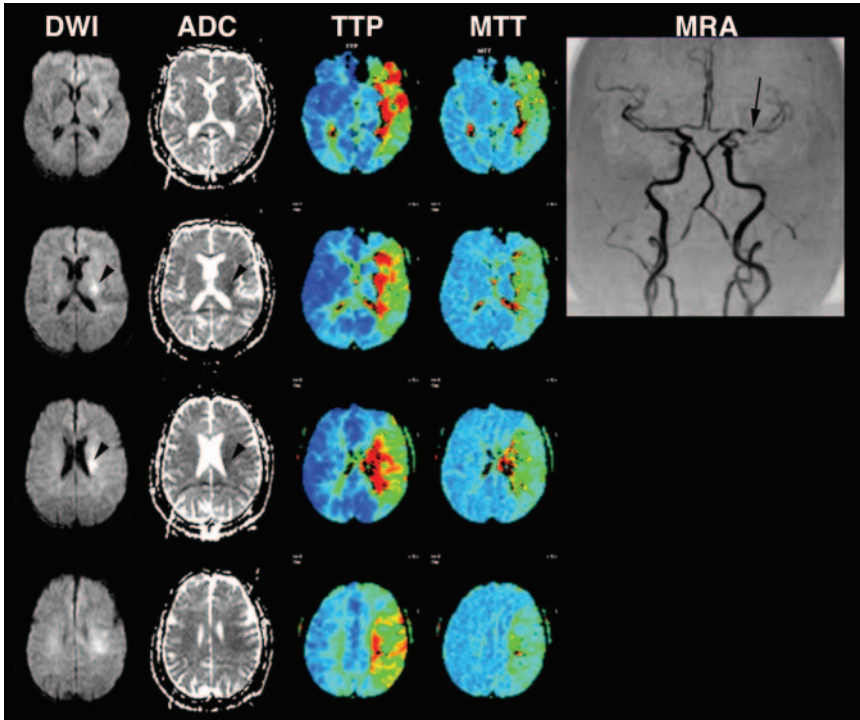
Figure 5. A 64-year-old male patient admitted with aphasia and right-body motor deficit. Admission MRA shows a proximal stenosis of the left middle cerebral artery (MCA; arrow). DWI and apparent diffusion coefficient (ADC) maps feature a focus of restricted diffusion in the deep territory of MCA (arrowheads), consistent with acute stroke. TTP and MTT maps demonstrate an extensive alteration of brain hemodynamics. The DWI–perfusion-weighted imaging mismatch is classically considered as a hallmark of tissue at risk or penumbra.

vessel occlusion on MRA, and absence of hemorrhage should prompt thrombolytic treatment[93–95] (Figure 5). DSC has also been used successfully to assess the cerebrovascular reserve[85,96] and vasospasm.[97]

In the management of patients with brain tumors, DSC can be combined with fine anatomic imaging, DWI, and spectroscopy, providing the most comprehensive information in one examination and leading to a high benefit/cost ratio.[98,99] DSC can differentiate high-grade glial tumors with neovascular proliferation and high CBV values with respect to low-grade glial tumors with low CBV. DSC can also evaluate the response to treatment (CBV decrease), differentiate tumor recurrence (high CBV) from radiation necrosis (low CBV), and distinguish tumor (high CBV) from infection (low CBV, but depending on the etiology) or tumefactive multiple sclerosis lesions (low CBV).[100–102]

Arterial Spin Labeling
Emmanuel Barbier, PhD;
Greg Zaharchuk, MD, PhD

Technical Description
ASL, also referred to as arterial spin tagging, relies on the detection of magnetically labeled water. Once the magnetization of the inflowing water has been modified (generally inverted) upstream, it induces a small MR signal change downstream (a few percent of the tissue magnetization). Meanwhile, the magnetization of the perfusion tracer (ie, the labeled water) is rapidly relaxing: the return of the longitudinal magnetization toward its equilibrium values takes a few seconds in the best cases (time constant T_1).[103,104]

Numerous ways to do the spin labeling have been described.[105–107] The existing techniques can be sorted out in 2
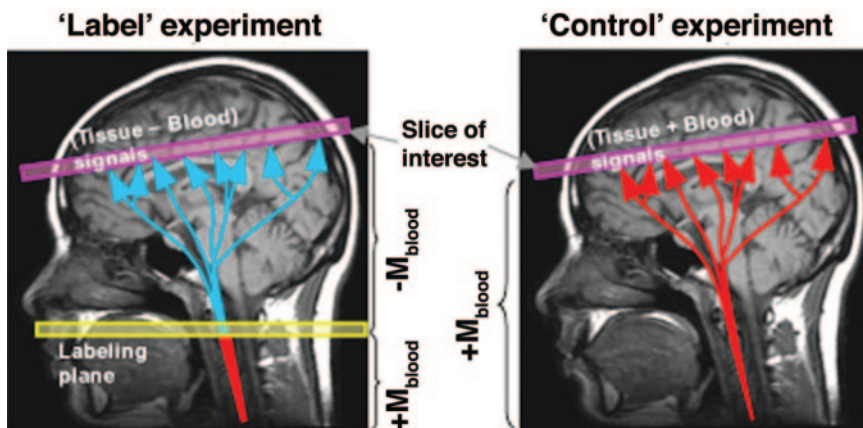
Figure 6. Principle of ASL MRI perfusion imaging. For demonstration, the continuous labeling method is depicted. Two sets of images are acquired: one (on the left) in which water protons are inverted proximally to the imaged slice and one (on the right) in which they are not. Subtraction of these 2 images provides a map of the distribution of the labeled water, which may be converted into quantitative CBF. Because the difference between the "label" and "control" images is on the order of 1% of the baseline images, multiple image pairs are collected and their signals summed to achieve adequate signal-to-noise. A typical ASL image at 1.5 T requires 5 to 10 minutes to acquire.

categories: pulsed techniques and continuous techniques, depending on how the spin labeling is performed. In both cases, a certain amount of blood magnetization is labeled before it irrigates the tissue of interest. With a "pulsed labeling" technique, the labeling is obtained by inverting the blood water magnetization in a thick slab of tissue located next to the slices of interest using a short (a few milliseconds) shaped radio frequency (RF) pulse. To better define the tail of this inverted blood bolus, a saturation pulse can be used advantageously.[108] With a "continuous labeling" technique (Figure 6), the labeling is performed continuously (during a few seconds) at the level of a plane through which blood flows (for the brain, this plane is located at the carotid level) either with the same coil or with a separate RF coil.[109] Finally, a recent approach has been proposed for which the blood magnetization is selectively inverted based on the blood velocity. This new pulsed technique differs from the classical pulse inversion and opens a new range of possibilities.[110,111]

The different ASL techniques share one characteristic: no contrast media is needed. ASL uses endogenous water as a tracer. A typical acquisition lasts between 5 and 10 minutes depending on the scanner quality (magnetic field, RF coil sensitivity, etc). Multiple pairs of label and control images are averaged together to obtain the required signal-to-noise ratio.

Technical Requirements

Performed in MRI scanners, ASL requires that the subject can be placed in a magnetic field, and hence patients are subject to MRI contraindications. Because ASL is a subtraction technique, it is very sensitive to subject movement. Recently, background suppression techniques have been proposed in which the static tissue signal is reduced as far as possible. In these approaches, the sensitivity of the technique to motion is greatly reduced.[112,113]

Interpretation

For pulsed and continuous technique types, a control acquisition is necessary. The control acquisition has to yield the same tissue signal but without inverting the blood magnetization. A simple subtraction between the averaged control and label images yields a flow-weighted map. Various models have been proposed to convert this flow-weighted image into a quantitative perfusion map. The data processing can be performed within a few minutes.[103,114–116]

The quantitative accuracy of the ASL technique has been addressed extensively in the literature. Computer simulations using an extensive model[117] and direct comparisons with other, non-nuclear MR, methods have been performed.[115,116,118,119] It appears that blood flow is correctly estimated in the gray matter. In white matter, numerical simulations predict an overestimation, whereas direct measurements show an underestimation. Quantitative ASL perfusion maps show a <10% change when rescanning the same subject.[120]

The difference in signal between the label and control acquisitions is ≈1% of the control images. Therefore, perfusion monitoring using ASL requires a very high signal-to-noise ratio. Because the signal difference is low, ASL cannot accurately map blood flow below ≈10 mL/100 g per minute. On the other hand, as flow increases (>150 mL/100 g per minute), ASL will underestimate blood flow. This is attributable in part to the fact that the labeled blood leaves the voxel (reduced extraction fraction) because this can be observed in animal models.[121]

In ASL techniques, the MRI sequences include spoiler gradients that suppress the signal arising from large vessels. Hence, ASL is not sensitive to large arteries or veins. The signal obtained with ASL comes mainly from water located in small vessels and in the surrounding tissue because of the water exchange between blood and tissue.[122]

In case of cerebrovascular disease, in which the time for blood to travel from the labeling plane to the imaged plane is longer and may be spatially heterogeneous, special methods involving long postlabeling delay times[123] or acquisition of images at multiple inversion times have to be implemented.[121] Even so, in the case of very long arrival times (eg, when flow is provided by collateral networks), the magnetic label of the blood may essentially be completely relaxed, such that no information about perfusion can be reliably ascertained.[124]

Feasibility

ASL examinations can be performed on any patient that can tolerate MRI. It is of particular interest for imaging CBF in infants and children, given the lack of ionizing radiation or need for intravenous access.

Perfusion maps obtained with ASL can cover the entire brain. In humans, the typical voxel size is 2×2×4 mm or 4×4×8 mm. Because fast imaging techniques are generally used, it can be challenging to obtain a good image quality in regions with strong magnetic susceptibility gradients (ie, magnetic field distortions), such as the base of the brain near the frontal sinuses.

Successive ASL CBF maps can be acquired every other 5 to 8 seconds. Thus, ASL techniques can be used successfully for functional MRI applications, in which control and label images are alternatively acquired.[125–127]

Clinical Applications

Although ASL techniques have not entered widespread clinical usage, their utility has been demonstrated for a variety of acute and chronic cerebrovascular diseases. ASL is feasible for acute stroke patients and other emergency patients in hospitals with MRI access, assuming that they are stable enough to undergo an MRI examination.

Initial studies were performed in the setting of ischemic cerebrovascular disease (stroke and transient ischemic attack), which demonstrated the feasibility of acquiring CBF maps using ASL in the acute and chronic settings.[128,129] Continuous ASL measurement of CBF reduction in the symptomatic hemisphere were shown to have high correlation with National Institutes of Health Stroke score.[130] ASL has also been used to study temporal lobe epilepsy[129] and brain tumor perfusion. A study of malignant gliomas demonstrated ASL perfusion imaging to be equally effective in determining tumor grade compared with DSC.[131]

One significant advantage of ASL is the ability to perform multiple repeated measurements, which might be necessary
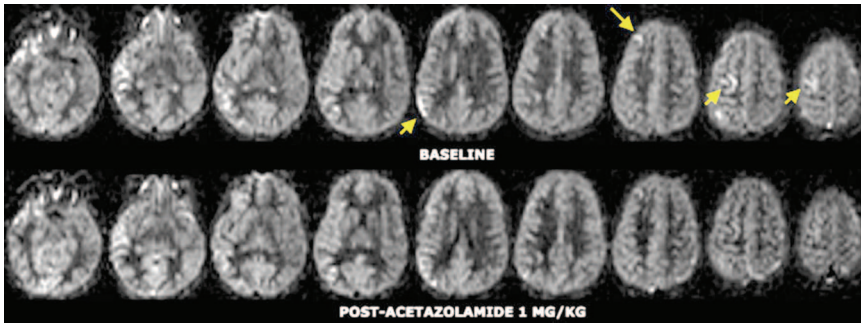
Figure 7. Preacetazolamide and postacetazolamide ASL CBF images of a 9-year-old girl with vasculitis, high-grade right-proximal ICA stenosis, and multiple subacute strokes (arrow). Significant CBF decrease is noted in the entire right hemisphere after acetazolamide, indicative of cerebrovascular steal. The effect is particularly marked in the regions of the subacute strokes.

before and after a cerebrovascular dilator (such as acetazolamide;[132] Figure 7) or before and after a neurointerventional procedure (such as carotid endarterectomy[133] or stenting). ASL methods also afford evaluation of functional brain activation,[134] useful, for instance, for the planning of neurosurgical procedures.

Doppler Ultrasound for Blood Flow Volume Measurement in ICAs
Jean-François Soustiel, MD; Thomas C. Glenn, MD

Technical Description

Numerous studies have shown the potential benefit of Doppler ultrasound–related techniques for the investigation of cerebral hemodynamics. Although different in nature from other imaging techniques described hereby and accordingly limited for spatial resolution, Doppler ultrasound offers the advantage of being noninvasive and can be repeated as often as clinically indicated at the patient's bedside. It does not involve radiation, does not require any contrast medium, and is free of any known adverse effect. In this regard, ultrasound Doppler technology may represent a convenient tool for the measurement of blood flow volume (BFV) in the ICA as a correlate for CBF in the corresponding hemisphere. Optimal BFV measurements of both ICAs are typically achieved within 10 to 20 minutes.[135,136]

Technical Requirements

This technique, although implemented in most commercial Duplex machines since the early 1990s,[135,136] has not initially gained wide acceptance because of significant inaccuracy inherent to errors caused by the impact of angle dependency on flow velocity and that of pulsatility on vessel diameter.[137–139] More recently, improvement in BFV measurement accuracy was achieved by combination of digital Doppler ultrasound and angle-independent dual-beam flow technology. This combination proved to be useful to overcome technical shortcomings of Doppler, such as angle dependency and time-dependent variations in velocity profile and vascular diameter.[140–143] These requirements are achieved, for instance, with the Quantix-ND system (Cardiosonix-Neoprobe), which uses pulse-wave digital Doppler to integrate with high-resolution temporal and spatial variations commonly overlooked by duplex imaging.[141,143]

Interpretation

Angle-independent dual-beam flow is based on the simultaneous use of 2 ultrasound beams with a known geometrical configuration. Using dedicated digital Doppler technology, hundreds of sample volumes of <200 μm in length at successive depths are simultaneously sampled along each ultrasound beam. Full fast Fourier transform analysis for each sample volume and application of an original algorithm allow real-time detection of flow velocity in the set of successive gates, followed by the determination of the chord segments that each beam traverses within the blood vessel. Because the angle between the 2 beams is known, the insonation angles of the 2 beams can be drawn from simple calculation based on trigonometric and Doppler considerations.[143] Further process-
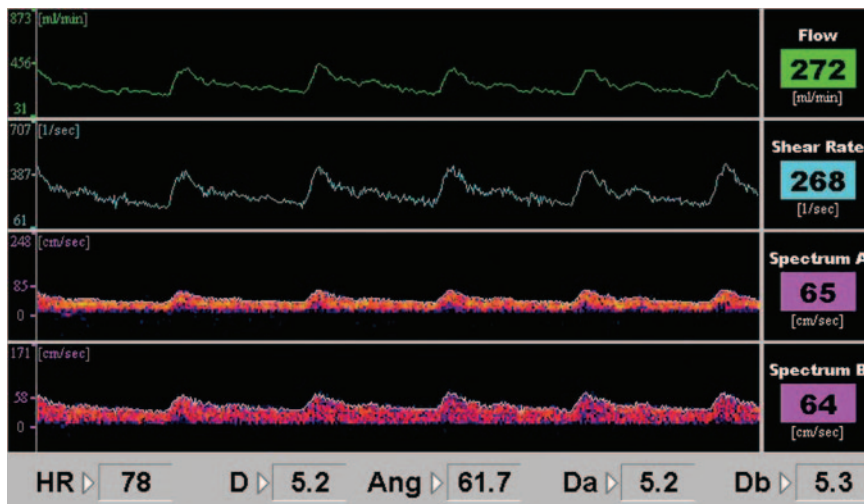
Figure 8. Graphic user interface of a computer system after a typical ICA BFV measurement. Along with flow data, spectra of both channels (spectrum A and spectrum B) with corresponding flow velocities (Flow) and diameters (Da and Db) are displayed to assess during the test and thereafter the adequate alignment of the ultrasound beam along the vessel axis, which represents a critical condition for accurate measurements. Note the optimal matching of velocities and diameters in this case. HR indicates heart rate; Ang, angle.

TABLE 2.   Main Strengths and Weaknesses of the Imaging Techniques Dedicated to Brain Hemodynamics

	Brain Perfusion Imaging Techniques						
	PET	SPECT	XeCT	PCT	DSC	ASL	Doppler
Main strengths	Accurate quantitative measurements	Technetium generator widely available	Accurate quantitative measurements	Wide availability of necessary equipment, including in the emergency setting	Can be combined with fine anatomic imaging, DWI, MRA, spectroscopy, providing the most comprehensive information in one examination	Repeatability (attributable to a lack of ionizing radiation)	Can be performed at bedside
	Assessment of multiple factors using various radioligands	Can be used at bedside and in the emergency setting	Assessment of multiple brain levels	Access to multiple perfusion parameters (CBV, CBF, MTT)	Repeatability (attributable to a lack of ionizing radiation)	Noninvasiveness (no intravenous injections)	Repeatability (attributable to a lack of ionizing radiation)
	Repeated measurements possibly attributable to short half-life of radiotracers	Low cost	Can be repeated at 10-minute intervals providing an ability to measure the CBF response to interventions	Accurate quantitative measurements	Whole brain coverage	flexibility (spatial resolution and imaging time can be traded off depending on the clinical question)	Noninvasiveness (no intravenous injections)
Main weaknesses	Impossible to use in the emergency settings	Relative, not quantitative measurements	Relatively long acquisition time, prone to motion artifacts	Presently limited anatomic coverage	Lack of standardization in the interpretation	CBF underestimation associated with extremely delayed arterial arrival times (such as through collateral pathways)	Provides only one value for each brain hemisphere
	High cost (however, cost-effective in well-established diagnostic algorithms)	Poor spatial resolution	Inhalation of Xenon via a face mask	use of ionizing radiation and iodinated contrast media	Not available in the emergency settings in most institutions	Relatively low signal-to-noise ratio per unit time	Operator dependent
			Xenon not currently approved by the FDA (technology only available at this time under IND status)		Difficulties associated with obtaining MRI (claustrophobia, contraindications, and access issues)	Difficulties associated with obtaining MRI (claustrophobia, contraindications, and access issues)	

ing of the large number of small sample volumes allows determination of the pulsatile velocity profile and vascular diameter. Determination of the insonation angles allows calculation of absolute blood flow velocities so that BFV can be directly obtained through integration of the velocity profile across the vascular cross-sectional area. BFV levels can be calculated online and displayed on a monitor (Figure 8) without any data postprocessing needed.

BFV measurements in the ICA may be used for the assessment of hemispheric or global CBF. Indeed, it shows a close and linear correlation with CBF in the corresponding hemisphere measured with ^{133}Xe clearance technique.[144,145] Admittedly, hemispheric CBF is not actually measured but estimated by BFV in the corresponding ICA based on the correlation between both parameters. Because this correlation is based on ICA BFV measurements, averaged CBF should not be confused with global blood flow because BFV in the vertebrobasilar system is not taken into consideration.

Attention should be paid, as for any Doppler-based technique, to minimize user-related variations and errors. Accordingly, examination review should take into consideration the quality of the obtained signal and discard any recorded data compromised by artifacts. In particular, insonation angle should be kept between 55° and 65° induced. Further, discrepancies between the 2 channel measurements of diameter should be kept at <0.5 mm for ICA diameter and at 20% for ICA flow velocities. Under these conditions, reproduc-

ibility of the measurements has proved to be satisfactorily low with interobserver variations ranging from 2.7% to 5.2%.

Feasibility

Doppler ultrasound is noninvasive and can be easily performed at patients' bedside for adults and children. Examinations can be obtained repeatedly or even set to a monitoring mode that may be critical in clinical situations characterized by dynamic changes. Yet improvement of temporal resolution is balanced by limited spatial resolution because BFV measurements performed on each ICA are related to hemispheric CBF, allowing only side-to-side difference analysis. Accordingly, focal CBF impairments confined to a rather small area or secondary to single vessel pathology may be masked by a remaining and otherwise preserved hemispheric flow.[143]

Clinical Applications

BFV measurements in the ICA represent a convenient tool for a bedside evaluation of hemispheric and global CBF. The high flexibility of this technique allows the operator to fit without interference within the busy environment of an intensive care unit or emergency room and obtain real-time data on CBF dynamics of unstable patients.

BFV measurements in the ICA may represent a potentially useful tool for the investigation of vasomotor response as part of the evaluation of cerebral occlusive disease and stroke instead of less accurate transcranial Doppler.[141] BFV measurements of extracranial vessels may be of benefit to provide additional objective information about the cerebral hemodynamic effects of ICA occlusion.[146–148] BFV measurements are also useful to detect CBF impairment attributable to either increased intracranial pressure or vasospasm after traumatic brain injuries and subarachnoid hemorrhage, respectively.[144] In these critically ill patients, clinical changes may develop rapidly and therefore be overlooked by sparsely performed CBF imaging studies. Further evaluations of drugs influencing CBF such as anesthetics, mannitol, and antihypertensive agents or any therapeutic measure may be of utmost importance for decision making, implying repeated CBF measurements within a short time. BFV measurements in the ICA adequately fulfill all these requirements.

Conclusion

Imaging techniques dedicated to brain perfusion all address the same types of pathological conditions, each having its own advantages and drawbacks (Table 2). PET is quantitatively accurate but feasible only in very specific settings. Its main application at the present time is its use for selection of patients with chronic ICA occlusion for bypass surgery. XeCT, on the other hand, is a reproducible quantitative technique that can be more easily used in the current clinical settings. It has classically been used for challenges such as acetazolamide. The main limitation of XeCT is that Xenon is not currently approved by the FDA and is available at this time only under IND status. Doppler ultrasound is the easiest technique to perform at bedside and is consequently used in numerous institutions as the primary tool to assess brain hemodynamics. Its main drawback lies in the fact that it does not provide values for each brain region (but only 1 value for

each supplying vessel or each hemisphere). To a certain extent, SPECT can also be performed at bedside: the radiopharmaceutical can be administered at the moment of the acute event, typically the seizure, and imaging is performed later, after stabilization of the patient, to identify the active epileptic focus. Among SPECT tracers, ^{133}Xe is not only historically the most important method for measuring brain hemodynamics but is still used as a gold standard in many hospitals that do not have PET. Doppler ultrasound and ASL do not use any contrast medium and do not require radiation. They can be used repeatedly and, hence, are useful for intensive care monitoring (for Doppler ultrasound that can be performed at bedside) or functional imaging (for ASL). PCT technique can be performed on conventional CT scanners and, as such, represents an ideal technique for ED patients, including stroke patients and head trauma patients. Finally, DSC can be combined with other MRI sequences, such as fine anatomic imaging, DWI, spectroscopy, etc, to provide the most comprehensive information in one examination and leading to a high benefit/cost ratio.

In conclusion, all imaging techniques dedicated to brain hemodynamics have their own advantages in specific clinical settings. The selection of one over another technique depends on the intrinsic characteristics pertaining to each imaging technique but also on the settings and on the knowledge and experience of institution staff.

References

1. Stewart GN. Researches on the circulation time and on the influences which affect it. V. The circulation time of the spleen, kidney, intestine, heart (coronary circulation) and retina, with some further observations on the time of the lesser circulation *Am J Physiol*. 1921;58:278–295.
2. Hamilton WF, Riley AM, Attyah AM. Comparison of the Fick and dye injection methods of measuring the cardiac output in man. *Am J Physiol*. 1948;153:309–321.
3. Kety SS, Schmidt CF. The nitrous oxide method for the quantitative determination of cerebral blood flow in man: theory, procedure and normal values. *J Clin Invest*. 1948;27:476–483.
4. Meier P, Zierler KL. On the theory of the indicator-dilution method for measurement of blood flow and volume. *J Appl Physiol*. 1954;6: 731–744.
5. Herscovitch P, Markham J, Raichle ME. Brain blood flow measured with intravenous H$_2$^{15}O. I. Theory and error analysis. *J Nucl Med*. 1983;24:782–789.
6. Raichle ME, Martin WRW, Herscovitch P, Mintun MA, Markham J. Brain blood flow measured with intravenous H$_2$^{15}O. II. Implementation and validation. *J Nucl Med*. 1983;24:790–798.
7. Jones T, Chesler DA, Ter-Pogossian MM. The continuous inhalation of oxygen-15 for assessing regional oxygen extraction in the brain of man. *Br J Radiol*. 1976;49:339–343.
8. Ibaraki M, Shimosegawa E, Miura S, Takahashi K, Ito H, Kanno I, Hatazawa J. PET measurements of CBF, OEF, and CMRO2 without arterial sampling in hyperacute ischemic stroke: method and error analysis. *Ann Nucl Med*. 2004;18:35–44.
9. Grubb R, Raichle M, Higins C, Eichling J. Measurement of regional cerebral blood flow by positron emission tomography. *Ann Neurol*. 1978;4:322–328.
10. Frakowiak RS, Lenzi GL, Jones T, Heather JD. Quantitative measurement of regional cerebral blood flow and oxygen metabolism in man using ^{15}O and positron emission tomography: Theory, procedure, and normal values. *J Comput Assist Tomogr*. 1980;4:727–736.
11. Phelps ME, Huang SC, Hoffman EJ, Selin C, Sokoloff L, and Kuhl DE. Tomographic measurement of local cerebral glucose metabolic rate in humans with (F-18)2-fluoro-2-deoxy-D-glucose: validation of method. *Ann Neurol*. 1979;6:371–388.
12. Reivich M, Kuhl D, Wolf A, Greenberg J, Phelps M, Ido T, Casella V, Fowler J, Hoffman E, Alavi A, Som P, Sokoloff L. The ^{18}F fluorode-

oxyglucose method for the measurement of local cerebral glucose utilization in man. *Circ Res*. 1979;44:127–137.

13. Nariai T, Senda M, Ishii K, Maehara T, Wakabayashi S, Toyama H, Ishiwata K, Hirakawa K. Three-dimensional imaging of cortical structure, function and glioma for tumor resection. *J Nucl Med*. 1997; 38:1563–1568.

14. Raichle ME. Quantitative in vivo autoradiography with positron emission tomography. *Brain Res*. 1979;180:47–68.

15. Fox PT, Mintun MA, Raichle ME, Herscovitch P. A noninvasive approach to quantitative functional brain mapping with H₂ (15)O and positron emission tomography. *J Cereb Blood Flow Metab*. 1984;4: 329–333.

16. Grubb RL Jr, Derdeyn CP, Fritsch SM, Carpenter DA, Yundt KD, Videen TO, Spitznagel EL, Powers WJ. Importance of hemodynamic factors in the prognosis of symptomatic carotid occlusion. *J Am Med Assoc*. 1998;280:1055–1060.

17. Derdeyn CP, Videen TO, Yundt KD, Fritsch SM, Carpenter DA, Grubb RL, Powers WJ. Variability of cerebral blood volume and oxygen extraction: stages of cerebral homodynamic impairment revisited. *Brain*. 2002;125:595–607.

18. Nariai T, Matsushima Y, Imae S, Tanaka Y, Ishii K, Senda M, Ohno K. Severe hemodynamic stress in selected subtypes of patients with moyamoya disease: a positron emission tomography study. *J Neurol Neurosurg Psychiatry*. 2005;76:663–669.

19. Nariai T, Senda M, Ishii K, Wakabayashi S, Yokota T, Toyama H, Matsushima Y, Hirakawa K. Posthyperventilatory steal response in chronic cerebral hemodynamic stress: a positron emission tomography study. *Stroke*. 1998;29:1281–1292.

20. Nariai T, Suzuki R, Hirakawa K, Maehara T, Ishii K, Senda M. Vascular reserve in chronic cerebral ischemia measured by the acetazolamide challenge test: comparison with positron emission tomography. *AJNR*. 1995;16:563–570.

21. Warwick JM. Imaging of brain function using SPECT. *Metab Brain Dis*. 2004;19:113–123.

22. Obrist WD, Thompson HK Jr, King CH, Wang HS. Determination of regional cerebral blood flow by inhalation of 133-Xenon. *Circ Res*. 1967;20:124–135.

23. Groch MW, Erwin WD. Single-photon emission computed tomography in the year 2001: instrumentation and quality control. *J Nucl Med Technol*. 2001;29:12–18.

24. Seret A, Defrise M, Blocklet D. 180 degree pinhole SPET with a tilted detector and OS-EM reconstruction: phantom studies and potential clinical applications. *Eur J Nucl Med*. 2001;28:1836–1841.

25. Lassen NA, Andersen AR, Friberg L, Paulson OB. The retention of ⁹⁹ᵐTc-d,l-HM-PAO in the human brain after intracarotid bolus injection: A kinetic analysis. *J Cereb Blood Flow Metab*. 1988;8:S13–S27.

26. Berrouschot J, Barthel H, Hesse S, Koster J, Knapp WH, Scheider D. Differentiation between transient ischemic attack and ischemic stroke within the first six hours after onset of symptoms by using ⁹⁹ᵐTc-ECD-SPECT. *J Cereb Blood Flow Metab*. 1998;18:921–929.

27. Alexandrov AV, Ehrlich LE, Bladin CF, Norris JW. Simple visual analysis of brain perfusion on HMPAO SPECT predicts early outcome in acute stroke. *Stroke*. 1996;27:1537–1542.

28. Ueda T, Sakaki S, Kumon Y, Ohta S. Multivariable analysis of predictive factors related to outcome at 6 months after intra-arterial thrombolysis for acute ischemic stroke. *Stroke*. 1999;30:2360–2365.

29. Alexandrov AV, Masdeu JC, Devous MD Sr, Black SE, Grotta JC. Brain single-photon emission CT with HMPAO and safety of thrombolytic therapy in acute ischemic stroke. *Stroke*. 1997;28:1830–1834.

30. Cikrit DF, Dalsing MC, Harting PS, Burt RW, Lalka SG, Sawchuk AP, Solooki B. Cerebral vascular reactivity assessed with acetazolamide single photon emission computer tomography scans before and after carotid endarterectomy. *Am J Surg*. 1997;174:193–197.

31. Cikrit DF, Dalsing MC, Lalka SG, Burt RW, Sawchuk AP, Solooki BA. The value of acetazolamide single photon emission computed tomography scans in the preoperative evaluation of asymptomatic critical carotid stenosis. *J Vasc Surg*. 1999;30:599–605.

32. Asenbaum S, Baumgartner C. Nuclear medicine in the preoperative evaluation of epilepsy. *Nucl Med Commun*. 2001;22:835–840.

33. Madeau JC, Abdel-Dayem H, Van Heertum RL. Head trauma: use of SPECT. *J Neuroimaging*. 1995;5(suppl 1):S53–S57.

34. Abdel-Dayem HM, Abu-Judeh H, Kumar M, Atay S, Naddaf S, El-Zeftawy H, Luo JQ. SPECT brain perfusion abnormalities in mild or moderate traumatic brain injury. *Clin Nucl Med*. 1998;23:309–317.

35. Buttler CRE, Costa DC, Walker Z, Katona CLE. PET and SPECT imaging in the dementias. In: Murray IPC, Ell PJ, eds. *Nuclear Medicine in Clinical Diagnosis and Treatment*. 2nd ed. Edinburgh, UK: Churchill Livingstone; 1998:713–728.

36. Ryding E. SPECT measurements of brain function in dementia: a review. *Acta Neurol Scand Suppl*. 1996;168:54–58.

37. Launes J, Siren J, Valanne L, Salonen O, Nikkinen P, Seppalainen AM, Liewendahl K. Unilateral hyperperfusion in brain-perfusion SPECT predicts poor prognosis in acute encephalitis. *Neurology*. 1997;48: 1347–1351.

38. Kao CH, Chan JL, ChangLai SP, Liao KK, Chieng PU. The role of FDG-PET, HMPAO-SPECT and MRI in the detection of brain involvement in patients with systemic lupus erythematosus. *Eur J Nucl Med*. 1999;26:129–134.

39. Weckesser M, Schober O. Brain death revisited: utility confirmed for nuclear medicine. *Eur J Nucl Med*. 1999;26:1387–1391.

40. Drayer BP, Wolfson SK, Reinmuth OM, Dujovny M, Boehnke M, Cook EE. Xenon-enhanced CT for analysis of cerebral integrity, perfusion, and blood flow. *Stroke*. 1978;9:123–130.

41. Kelcz F, Hilal SK, Hartwell P, Joseph PM. Computed tomographic measurement of the xenon brain-blood partition coefficient and implications for regional blood flow: a preliminary report. *Radiology*. 1978; 127:385–392.

42. Von Oettingen G, Bergholt B, Rasmussen M, Ostergaard L, Astrup J. Pulmonary function affects the quantification of CBF by non-invasive xenon methods. *J Neurosci Methods*. 2000;95:159–169.

43. Good WF, Gur D, Yonas H. In: Yonas H, ed. *Cerebral Blood Flow Measurements With Stable Xenon-Enhanced Computed Tomography: Technical Aspects*. New York, NY: Raven Press Ltd; 1992:4–15.

44. Latchaw RE, Yonas H, Pentheny SL, Gur D. Adverse reactions to xenon-enhanced CT cerebral blood flow determination. *Radiology*. 1987;163:251–254.

45. Latchaw RE, Yonas H, Hunter GJ, Yuh WT, Ueda T, Sorensen AG, Sunshine JL, Biller J, Wechsler L, Higashida R, Hademenos G; Council on Cardiovascular Radiology of the American Heart Association. Guidelines and recommendations for perfusion imaging in cerebral ischemia. *Stroke*. 2003;34:1084–1104.

46. Gur D, Good WF, Wolfson SK, Yonas H, Shabason L. In vivo mapping of local cerebral blood flow by xenon-enhanced computed tomography. *Science*. 1982;215:1267–1268.

47. Pindzola RR, Yonas. The xenon-enhanced computed tomography cerebral blood flow method. *Neurosurgery*. 1998;43:1488–1492.

48. Obrist WD, Zhang Z, Yonas H. Effect of xenon-induced flow activation on xenon-enhanced computed tomography cerebral blood flow calculations. *J Cereb Blood Flow Metab*. 1998;18:1192–1195.

49. Firlik AD, Rubin G, Yonas H, Wechsler LR. Relation between cerebral blood flow and neurologic deficit resolution in acute ischemic stroke. *Neurology*. 1998;51:177–182.

50. Field M, Jungreis CA, Chengelis N, Kromer H, Kirby L, Yonas H. Symptomatic cavernous sinus aneurysms: Management and outcome after carotid occlusion and selective cerebral revascularization. *AJNR*. 2003;24:1200–1207.

51. McLaughlin MR, Marion DW. Cerebral blood flow and vasoresponsivity within and around cerebral contusions. *J Neurosurg*. 1996;85: 871–876.

52. Yonas H, Smith HA, Durham SR, Pentheny SL, Johnson DW. Increased stroke risk predicted by compromised cerebral blood flow reactivity. *J Neurosurg*. 1993;79:483–489.

53. Darby JM, Yonas H, Marks EC, Durham S, Snyder RW, Nemoto EM. Acute cerebral blood flow response to dopamine-induced hypertension after subarachnoid hemorrhage. *J Neurosurg*. 1994;80:857–864.

54. Adelson PD, Clyde B, Kochanek PM, Wisniewski SR, Marion DW, Yonas H. Cerebrovascular response in infants and young children following severe traumatic brain injury: a preliminary report. *Pediatr Neurosurg*. 1997;26:200–207.

55. Eastwood JD, Lev MH, Provenzale JM. Perfusion CT with iodinated contrast material. *AJR Am J Roentgenol*. 2003;180:3–12.

56. Wintermark M, Maeder P, Verdun FR, Thiran JP, Valley JF, Schnyder P, Meuli R. Using 80 kVp versus 120 kVp in perfusion CT measurement of regional cerebral blood flow. *AJNR*. 2000;21:1881–1884.

57. Smith WS, Roberts HC, Chuang NA, Ong KC, Lee TJ, Johnston SC, Dillon WP. Safety and feasibility of a CT protocol for acute stroke: combined CT, CT angiography, and CT perfusion imaging in 53 consecutive patients. *AJNR*. 2003;24:688–690.

58. Wintermark M, Smith WS, Ko NU, Quist M, Schnyder P, Dillon WP. Dynamic perfusion CT: optimizing the temporal resolution and contrast volume for calculation of perfusion CT parameters in stroke patients. *AJNR*. 2004;25:720–729.

59. Wintermark M, Maeder P, Thiran JP, Schnyder P, Meuli R. Quantitative assessment of regional cerebral blood flows by perfusion CT studies at low injection rates: a critical review of the underlying theoretical models. *Eur Radiol*. 2001;11:1220–1230.

60. Kudo K, Terae S, Katoh C, Oka M, Shiga T, Tamaki N, Miyasaka K. Quantitative cerebral blood flow measurement with dynamic perfusion CT using the vascular-pixel elimination method: comparison with H$_2$(15)O positron emission tomography. *AJNR*. 2003;24:419–426.

61. Eastwood JD, Lev MH, Wintermark M, Fitzek C, Barboriak DP, Delong DM, Lee TY, Azhari T, Herzau M, Chilukuri VR, Provenzale JM. Correlation of early dynamic CT perfusion imaging with whole-brain MR diffusion and perfusion imaging in acute hemispheric stroke. *AJNR*. 2003;24:1869–1875.

62. Eastwood JD, Lev MH, Azhari T, Lee TY, Barboriak DP, Delong DM, Fitzek C, Herzau M, Wintermark M, Meuli R, Brazier D, Provenzale JM. CT perfusion scanning with deconvolution analysis: pilot study in patients with acute middle cerebral artery stroke. *Radiology*. 2002;222: 227–236.

63. Wintermark M, Reichhart M, Cuisenaire O, Maeder P, Thiran JP, Schnyder P, Bogousslavsky J, Meuli R. Comparison of admission perfusion computed tomography and qualitative diffusion- and perfusion-weighted magnetic resonance imaging in acute stroke patients. *Stroke*. 2002;33:2025–2031.

64. Wintermark M, Reichhart M, Thiran JP, Maeder P, Chalaron M, Schnyder P, Bogousslavsky J, Meuli R. Prognostic accuracy of cerebral blood flow measurement by perfusion computed tomography, at the time of emergency room admission, in acute stroke patients. *Ann Neurol*. 2002;51:417–432.

65. Wintermark M, Fischbein NJ, Smith WS, Ko NU, Quist M, Dillon WP. Accuracy of dynamic perfusion-CT with deconvolution in detecting acute hemispheric stroke. *AJNR*. 2005;26:104–112.

66. Eastwood JD, Alexander MJ, Petrella JR, Provenzale JM. Dynamic CT perfusion imaging with acetazolamide challenge for the preprocedural evaluation of a patient with symptomatic middle cerebral artery occlusive disease. *AJNR*. 2002;23:285–287.

67. Nabavi DG, LeBlanc LM, Baxter B, Lee DH, Fox AJ, Lownie SP, Ferguson GG, Craen RA, Gelb AW, Lee TY. Monitoring cerebral perfusion after subarachnoid hemorrhage using CT. *Neuroradiology*. 2001;43:7–16.

68. Wintermark M, Ko NU, Smith WS, Liu S, Higashida RT, Dillon WP. Vasospasm after subarachnoid hemorrhage: utility of Perfusion-CT and CT-Angiography on diagnosis and management. *AJNR*. In press.

69. Wintermark M, van Melle G, Schnyder P, Revelly JP, Porchet F, Regli L, Meuli R, Maeder P, Chiolero R. Admission perfusion CT: prognostic value in patients with severe head trauma. *Radiology*. 2004;232: 211–220.

70. Wintermark M, Chiolero R, van Melle G, Revelly JP, Porchet F, Regli L, Meuli R, Schnyder P, Maeder P. Relationship between brain perfusion computed tomography variables and cerebral perfusion pressure in severe head trauma patients. *Crit Care Med*. 2004;32:1579–1587.

71. Wintermark M, Bogousslavsky J. Imaging of acute ischemic brain injury: the return of computed tomography. *Curr Opin Neurol*. 2003; 16:59–63.

72. Rosen BR, Belliveau JW, Vevea JM, Brady TJ. Perfusion imaging with NMR contrast agents. *Magn Reson Med*. 1990;14:249–265.

73. Grandin CB. Assessment of brain perfusion with MRI: methodology and application to acute stroke. *Neuroradiology*. 2003;45:755–766.

74. Speck O, Chang L, DeSilva NM, Ernst T. Perfusion MRI of the human brain with dynamic susceptibility contrast: gradient-echo versus spin-echo techniques. *J Magn Reson Imaging*. 2000;12:381–387.

75. Harrer JU, Parker GJ, Haroon HA, Buckley DL, Embelton K, Roberts C, Baleriaux D, Jackson A. Comparative study of methods for determining vascular permeability and blood volume in human gliomas. *J Magn Reson Imaging*. 2004;20:748–757.

76. Jackson A, Kassner A, Annesley-Williams D, Reid H, Zhu XP, Li KL. Abnormalities in the recirculation phase of contrast agent bolus passage in cerebral gliomas: comparison with relative blood volume and tumor grade. *AJNR*. 2002;23:7–14.

77. Cha S. Perfusion MR imaging: basic principles and clinical applications. *Magn Reson Imaging Clin N Am*. 2003;11:403–413.

78. Østergaard L, Weisskoff RM, Chesler DA, Gyldensted C, Rosen RR. High resolution measurement of cerebral blood flow using intravascular tracer bolus passages. Part I: mathematical approach and statistical analysis. *Magn Reson Med*. 1996;36:715–725.

79. Smith AM, Grandin CB, Duprez T, Mataigne F, Cosnard G. Whole brain quantitative CBF and CBV measurements using MRI bolus tracking: comparison of methodologies. *Magn Reson Med*. 2000;43:559–564.

80. Østergaard L, Smith DF, Vestergaard-Poulsen P, Hansen SB, Gee AD, Gjedde A, Gyldensted C. Absolute cerebral blood flow and volume measured by magnetic resonance imaging bolus tracking: comparison with positron emission tomography values. *J Cereb Blood Flow Metab*. 1998;18:425–432.

81. Kiselev VG. On the theoretical basis of perfusion measurements by dynamic susceptibility contrast MRI. *Magn Reson Med*. 2001;46: 1113–1122.

82. Østergaard L, Johannsen P, Høst-Poulsen P, Vestergaard-Poulsen P, Asboe H, Gee AD, Hansen SB, Cold GE, Gjedde A, Gyldensted C. Cerebral blood flow measurements by magnetic resonance imaging bolus tracking: comparison with [^{15}O]H$_2$O positron emission tomography in humans. *J Cereb Blood Flow Metab*. 1998;18:935–940.

83. Hagen T, Bartylla K, Piepgras U. Correlation of regional cerebral blood flow measured by stable xenon CT and perfusion MRI. *J Comput Assist Tomogr*. 1999;23:257–264.

84. Sakoh M, Rohl L, Gyldensted C, Gjedde A, Østergaard L. Cerebral blood flow and blood volume measured by magnetic resonance imaging bolus tracking after acute stroke in pigs: comparison with [^{15}O]-H$_2$O positron emission tomography. *Stroke*. 2000;31:1958–1964.

85. Schreiber WG, Gükel F, Stritzke P, Schmiedek P, Schwartz A, Brix G. Cerebral blood flow and cerebrovascular reserve capacity: estimation by dynamic magnetic resonanace imaging. *J Cereb Blood Flow Metab*. 1998;18:1143–1156.

86. Grandin CB, Bol A, Smith AM, Michel C, Cosnard G. Absolute CBF and CBV measurements by MRI bolus tracking before and after acet-azolamide challenge: repeatability and comparison with PET in humans. *Neuroimage*. 2005;26:525–535.

87. Levin JM, Kaufman MJ, Ross MH, Mendelson JH, Maas LC, Cohen BM, Renshaw PH. Sequential dynamic susceptibility contrast MR experiments in human brain: residual contrast agent effect, steady state, and hemodynamic perturbation. *Magn Reson Med*. 1995;34:655–663.

88. Sorensen G, Copen WA, Østergaard L, Buonanno FS, Gonzalez RG, Rordorf G, Rosen BR, Schwamm RM, Weisskoff RM, Koroshetx WJ. Hyperacute stroke: simultaneous measurement of relatoive cerebral blood volume, relative cerebral blood flow, and mean tissue transit time. *Radiology*. 1999;210:519–527.

89. Thomalla GJ, Kucinski T, Schoder V, Fiehler J, Knab R, Zeumer H, Weiller C, Rother J. Prediction of malignant middle cerebral artery infarction by early perfusion- and diffusion-weighted magnetic resonance imaging. *Stroke*. 2003;34:1892–1899.

90. Gauvrit JY, Delmaire C, Henon H, Debette S, al Koussa M, Leys D, Pruvo JP, Leclerc X. Diffusion/perfusion-weighted magnetic resonance imaging after carotid angioplasty and stenting. *J Neurol*. 2004;251: 1060–1067.

91. Grandin CB, Duprez TP, Smith AM, Which M. R-derived perfusion parameters predict infarct growth the best in hyperacute stroke? A comparative study between relative and quantitative measurements. *Radiology*. 2002;223:361–370.

92. Shih LC, Saver JL, Alger JR, Starkman S, Leary MC, Vinuela F, Duckwiler G, Gobin P, Jahan R, Villablanca JP, Vespa PM, Kidwell CS. Perfusion-weighted magnetic resonance imaging thresholds identifying core, irreversibly infarcted tissue. *Stroke*. 2003;34:1425–1430.

93. Albers GW. Expanding the window for thrombolytic therapy in acute stroke. The potential role of acute MRI for patients selection. *Stroke*. 1999;30:2230–2237.

94. Schellinger PD, Fiebach JB, Hacke W. Imaging-based decision making in thrombolytic therapy for ischemic stroke: present status. *Stroke*. 2003;34:575–583.

95. Kidwell CS, Alger JR, Saver JL. Evolving paradigms in imaging the ischemic penumbra with multimodal magnetic resonance imaging. *Stroke*. 2004;35:2662–2665.

96. Gükel FJ, Brix G, Schmiedek P, Piepgras A, Becker G, Köpke J, Gross H, Georgi M. Cerebrovascular reserve capacity in patients with occlusive cerebrovascular disease: assessment with dynamic susceptibility contrast-enhanced MR imaging and the acetazolamide stimulation test. *Radiology*. 1996;201:405–412.

97. Rordorf G, Koroshetz WJ, Copen WA, Gonzalez G, Yamada K, Schaefer PW, Schwamm LH, Ogilvy CS, Sorensen AG. Diffusion- and perfusion-weighted imaging in vasospasm after subarachnoid hemorrhage. *Stroke*. 1999;30:599–605.

98. Yang D, Korogi Y, Sugahara T, Kitajima M, Shigematsu Y, Liang L, Ushio Y, Takahashi M. Cerebral gliomas: prospective comparison of multivoxel 2D chemical-shift imaging proton MR spectroscopy, echoplanar perfusion and diffusion-weighted MRI. *Neuroradiology*. 2002;44:656–666.

99. Law M, Yang S, Wang H, Babb JS, Johnson G, Cha S, Knopp EA, Zagzag D. Glioma grading: sensitivity, specificity, and predictive values of perfusion MR imaging and proton MR spectroscopic imaging compared with conventional MR imaging. *AJNR*. 2003;24:1989–1998.

100. Cha S, Knopp EA, Johnson G, Wetzel SG, Litt AW, Zagzag D. Intracranial mass lesions: dynamic contrast-enhanced susceptibility-weighted echo-planar perfusion MR imaging. *Radiology*. 2002;223:11–29.

101. Akella NS, Twieg DB, Mikkelsen T, Hochberg FH, Grossman S, Cloud GA, Nabors LB. Assessment of brain tumor angiogenesis inhibitors using perfusion magnetic resonance imaging: quality and analysis results of a phase I trial. *J Magn Reson Imaging*. 2004;20:913–922.

102. Holmes TM, Petrella JR, Provenzale JM. Distinction between cerebral abscesses and high-grade neoplasms by dynamic susceptibility contrast perfusion MRI. *AJR*. 2004;183:1247–1252.

103. Detre JA, Leigh JS, Williams DS, Koretsky AP. Perfusion imaging. *Magn Reson Med*. 1992;23:37–45.

104. Kwong KK, Chesler DA, Weisskoff RM, Donahue KM, Davis TL, Ostergaard L, Campbell TA, Rosen BR. MR perfusion studies with T1 weighted echo planar imaging, *Magn Reson Med*. 1995;34:878–887.

105. Calamante F, Thomas DL, Pell GS, Wiersma J, Turner R. Measuring cerebral blood flow using magnetic resonance imaging techniques. *J Cereb Blood Flow Metab*. 1999;19:701–735.

106. Golay X, Hendrikse J, Lim TC. Perfusion imaging using arterial spin labeling. *Top Magn Reson Imaging*. 2004;15:10–27.

107. Barbier EL, Lamalle L, Decorps M. Methodology of brain perfusion imaging. *J Magn Reson Imaging*. 2001;13:496–520.

108. Wong EC, Buxton RB, Frank LR. Quantitative imaging of perfusion using a single subtraction (QUIPSS and QUIPSS II). *Magn Reson Med*. 1998;39:702–708.

109. Zaharchuk G, Ledden PJ, Kwong KK, Reese TG, Rosen BR, Wald LL. Multislice perfusion and perfusion territory imaging in humans with separate label and image coils. *Magn Reson Med*. 1999;41:1093–1098.

110. Norris DG, Schwarzbauer C. Velocity selective radiofrequency pulse trains. *J Magn Reson*. 1999;137:231–236.

111. Duhamel G, de Bazelaire C, Alsop DC. Evaluation of systematic quantification errors in velocity-selective arterial spin labeling of the brain. *Magn Reson Med*. 2003;50:145–153.

112. Talagala SL, Ye FQ, Ledden PJ, Chesnick S. Whole-brain 3D perfusion MRI at 3.0 T using CASL with a separate labeling coil. *Magn Reson Med*. 2004;52:131–140.

113. Ye FQ, Frank JA, Weinberger DR, McLaughlin AC. Noise reduction in 3D perfusion imaging by attenuating the static signal in arterial spin tagging (ASSIST). *Magn Reson Med*. 2000;44:92–100.

114. McLaughlin AC, Ye FQ, Pekar JJ, Santha AK, Frank JA. Effect of magnetization transfer on the measurement of cerebral blood flow using steady-state arterial spin tagging approaches: a theoretical investigation. *Magn Reson Med*. 1997;37:501–510.

115. Ye FQ, Berman KF, Ellmore T, Esposito G, van Horn JD, Yang Y, Duyn J, Smith AM, Frank JA, Weinberger DR, McLaughlin AC. H(2)(15)O PET validation of steady-state arterial spin tagging cerebral blood flow measurements in humans. *Magn Reson Med*. 2000;44: 450–456.

116. Buxton RB, Frank LR, Wong EC, Siewert B, Warach S, Edelman RR. A general kinetic model for quantitative perfusion imaging with arterial spin labeling. *Magn Reson Med*. 1998;40:383–396.

117. St. Lawrence KS, Frank JA, McLaughlin AC. Effect of restricted water exchange on cerebral blood flow values calculated with arterial spin tagging: a theoretical investigation. *Magn Reson Med*. 2000;44: 440–449.

118. Ewing JR, Fenstermacher JD. The single-coil arterial spin-tagging experiment for estimating cerebral blood flow as viewed from the capillary. What is the effective T1 of the experiment? Philadelphia, Pa: ISMRM, 7th Annual Meeting, 1999:1846.

119. Ewing JR, Wei L, Knight R, Nagaraja TN, Fenstermacher JD. A direct comparison between MRI arterial spin-tagging and quantitative autoradiography for measured cerebral blood flow in rats with experimental

cerebral ischemia. Copenhagen: Brain'99, 19th Annual Meeting, 1999:595.

120. Parkes LM, Rashid W, Chard DT, Tofts PS. Normal cerebral perfusion measurements using arterial spin labeling: reproducibility, stability, and age and gender effects. *Magn Reson Med*. 2004;51:736–743.

121. Barbier EL, Silva AC, Kim SG, Koretsky AP. Perfusion imaging using dynamic arterial spin labeling (DASL). *Magn Reson Med*. 2001;45: 1021–1029.

122. Ye FQ, Mattay VS, Jezzard P, Frank JA, Weinberger DR, McLaughlin AC. Correction for vascular artifacts in cerebral blood flow values measured by using arterial spin tagging techniques. *Magn Reson Med*. 1997;37:226–237.

123. Alsop DC, Detre JA. Multisection cerebral blood flow MR imaging with continuous arterial spin labeling. *Radiology*. 1998;208:410–416.

124. Schepers J, Veldhuis WB, Pauw RJ, de Groot JW, van Osch MJ, Nicolay K, van der Sanden BP. Comparison of FAIR perfusion kinetics with DSC-MRI and functional histology in a model of transient ischemia. *Magn Reson Med*. 2004;51:312–320.

125. Wang J, Alsop DC, Li L, Listerud J, Gonzalez-At JB, Schnall MD, Detre JA. Comparison of quantitative perfusion imaging using arterial spin labeling at 1.5 and 4.0 Tesla. *Magn Reson Med*. 2002;48:242–254.

126. Detre JA, Wang J. Technical aspects and utility of fMRI using BOLD and ASL. *Clin Neurophysiol*. 2002;113:621–634.

127. Detre JA, Alsop DC. Perfusion magnetic resonance imaging with continuous arterial spin labeling: methods and clinical applications in the central nervous system. *Eur J Radiol*. 1999;30:115–124.

128. Detre JA, Alsop DC, Vives LR, Maccotta L, Teener JW, Raps EC. Noninvasive MRI evaluation of cerebral blood flow in cerebrovascular disease. *Neurology*. 1998;50:633–664.

129. Wolf RL, Alsop DC, McGarvey ML, Maldjian JA, Wang J, Detre JA. Susceptibility contrast and arterial spin label perfusion MRI in cerebrovascular disease. *J Neuroimaging*. 2003;13:17–27.

130. Chalela JA, Alsop DC, Gonzalez-Atavales JB, Maldjian JA, Kasner SE, Detre JA. Magnetic resonance perfusion imaging in acute ischemic stroke using continuous arterial spin labeling. *Stroke*. 2000;31:680–687.

131. Warmuth C, Gunther M, Zimmer C. Quantification of blood flow in brain tumors: comparison of arterial spin labeling and dynamic susceptibility-weighted contrast-enhanced MR imaging. *Radiology*. 2003;228:523–532.

132. Detre JA, Samuels OB, Alsop DC, Gonzalez-At JB, Kasner SE, Raps EC. Noninvasive magnetic resonance imaging evaluation of cerebral blood flow with acetazolamide challenge in patients with cerebrovascular stenosis. *J Magn Reson Imaging*. 1999;10:870–875.

133. Ances BM, McGarvey ML, Abrahams JM, Maldjian JA, Alsop DC, Zager EL, Detre JA. Continuous arterial spin labeled perfusion magnetic resonance imaging in patients before and after carotid endarterectomy. *J Neuroimaging*. 2004;14:133–138.

134. Silva AC, Kim S-G. Perfusion-based functional magnetic resonance imaging. *Concepts in Magn Reson Part A*. 2003;16A:16–27.

135. Schoning M, Walter J, Scheel P. Estimation of cerebral blood flow through color duplex sonography of the carotid and vertebral arteries in healthy adults. *Stroke*. 1994;25:17–22.

136. Leopold PW, Shandall AA, Feustel P, Corson JD, Shah DM, Popp AJ, Fortune JB, Leather RP, Karmody AM. Duplex scanning of the internal carotid artery: an assessment of cerebral blood flow. *Br J Surg*. 1987; 74:630–633.

137. Eicke BM, Kremkau FW, Hinson H, Tegeler CH. Peak velocity overestimation and linear-array spectral Doppler. *J Neuroimaging*. 1995;5: 115–121.

138. Steinman AH, Tavakkoli J, Myers JG Jr, Cobbold RS, Johnston KW. Sources of error in maximum velocity estimation using linear phased-array Doppler systems with steady flow. *Ultrasound Med Biol*. 2001;27:655–664.

139. Ho SSY, Metreweli C. Preferred technique for blood flow volume measurement in cerebrovascular disease. *Stroke*. 2000;31:1342–1345.

140. Rasmussen TE, Panneton JM, Kalra M, Hofer JM, Lewis BD, Rowland CM, Bower TC, Cherry KJ Jr, Noel AA, Gloviczki P. Intraoperative use of a new angle-independent Doppler system to measure arterial velocities after carotid endarterectomy. *J Vasc Surg*. 2003;37:374–380.

141. Schebesch KM, Simka S, Woertgen C, Brawanski A, Rothoerl RD. Normal values of volume flow in the internal carotid artery measured by a new angle-independent Doppler technique for evaluating cerebral perfusion. *Acta Neurochir (Wien)*. 2004;146:983–986.

142. Skladany M, Vilkomerson D, Lyons D, Chilipka T, Delamere M, Hollier LH. New, angle-independent, low cost Doppler system to measure blood flow. *Am J Surg*. 1998;176:179–182.

143. Soustiel JF, Levy E, Zaaroor M, Bibi R, Lukaschuk S, Manor D. A new angle-independent Doppler ultrasonic device for the assessment of blood flow volume in the extracranial internal carotid artery. *J Ultrasound Med*. 2002;21:1405–1412.

144. Rothoerl RD, Schebesch KM, Woertgen C, Brawanski A. Internal carotid artery volume flow correlates to rCBF measurements. *Acta Neurochir*. 2003;145:943–947.

145. Soustiel JF, Glenn TC, Vespa P, Rinsky B, Hanuscin C, Martin NA. Assessment of cerebral blood flow by means of blood-flow-volume measurement in the internal carotid artery: comparative study with a 133xenon clearance technique. *Stroke*. 2003;34:1876–1880.

146. Lam WW, Ho SS, Leung SF, Wong KS, Metreweli C. Cerebral blood flow measurement by color velocity imaging in radiation-induced carotid stenosis. *J Ultrasound Med*. 2003;22:1055–1060.

147. Niesen WD, Weiller C, Sliwka U. Unstable cerebral hemodynamics in carotid artery occlusion and large hemispheric stroke: a cerebral blood flow volume study. *J Neuroimaging*. 2004;14:246–250.

148. Tan TY, Schminke U, Lien LM, Eicke BM, Tegeler CH. Extracranial internal carotid artery occlusion: the role of common carotid artery volume flow. *J Neuroimaging*. 2002;12:144–147.